Theory of Electromagnons in the Multiferroic Mn Perovskites: The Vital Role of Higher Harmonic Components of the Spiral Spin Order

Masahito Mochizuki,[1,*] Nobuo Furukawa,[2,3] and Naoto Nagaosa[1,4]

[1]*Department of Applied Physics, The University of Tokyo, 7-3-1, Hongo, Bunkyo-ku, Tokyo 113-8656, Japan*
[2]*Department of Physics, Aoyama Gakuin University, Fuchinobe 5-10-1, Sagamihara, 229-8558 Japan*
[3]*Multiferroics Project, ERATO, Japan Science and Technology Agency (JST) c/o Department of Applied Physics, The University of Tokyo, Tokyo 113-8656, Japan*
[4]*Cross-Correlated Materials Research Group (CMRG) and Correlated Electron Research Group (CERG), RIKEN-ASI, Saitama 351-0198, Japan*

(Received 14 January 2010; published 30 April 2010)

We study theoretically the electromagnon and its optical spectrum (OS) of the terahertz-frequency regime in the magnetic-spiral-induced multiferroic phases of the rare-earth-metal (R) Mn perovskites, $R\mathrm{MnO_3}$, taking into account the spin-angle modulation or the higher harmonics of the spiral spin configuration, which has been missed so far. A realistic spin Hamiltonian, which gives phase diagrams in agreement with experiments, resolves a puzzle, i.e., the double-peak structure of the OS with a larger low-energy peak originating from magnon modes hybridized with the zone-edge state. We also predict the magnon branches associated with the electromagnon, which can be tested by neutron-scattering experiment.

DOI: 10.1103/PhysRevLett.104.177206 PACS numbers: 75.80.+q, 75.30.Ds, 75.40.Gb, 76.50.+g

The charge dynamics below the Mott gap in Mott insulators is an issue of intensive recent interest. The rich structures of the low-energy optical spectrum (OS) are associated with the spin degree of freedom in so-called multiferroics, which shows both magnetic and ferroelectric orders [1]. The spontaneous electric polarization ($\boldsymbol{P}$) in these materials is driven by the magnetic ordering, and the strong coupling between the dynamics of $\boldsymbol{P}$ and magnetism is inevitable. In particular, in the rare-earth-metal (R) perovskite manganites $R\mathrm{MnO_3}$ [2], which is the main target of this Letter, the relativistic spin-orbit interaction and the spin current play essential roles in the multiferroic behavior [3–5]. Excitations of the magnet are usually described as the spin wave or the magnon, i.e., a harmonic oscillation of spins around their ground-state configuration. It couples to $\boldsymbol{P}$ in the multiferroics, and thus is termed electromagnon [6]. It is crucial to understand the OS of the electromagnon to design the giant magnetoelectric (ME) coupling in the terahertz-frequency regime.

In $R\mathrm{MnO_3}$, frustration between the spin-exchange interactions leads to a noncollinear spin spiral in the ground state. This simple idea, however, cannot explain the rich phase diagrams in the plane of Mn-O-Mn bond angle and temperature, and also those under magnetic fields. In real systems, there are other interactions originating from the relativistic spin-orbit interaction such as the magnetic anisotropy and the Dzyaloshinskii-Moriya (DM) interaction. By studying a realistic spin Hamiltonian taking into account these interactions, the phase diagrams including the spin-flop transition have been understood except for the collinear E-type spin phase [7]. It turned out that the spin-phonon coupling or the resulting biquadratic interaction plays an important role in stabilizing the E-type phase [8], which is expected to play some roles even in the neighboring spiral phases.

On the other hand, after the first experimental observation of the terahertz OS in the multiferroic $R\mathrm{MnO_3}$ [9,10], it was interpreted as a collective mode corresponding to rotation of the spin-spiral plane associated with fluctuations of the $\boldsymbol{P}$ direction [11]. Later it turned out that the selection rule and the magnitude of oscillator strength ruled out this interpretation [12,13], and a new mechanism has been searched for. The most promising candidate is the conventional magnetostriction mechanism [14,15], where $\boldsymbol{P}$ is given by $\boldsymbol{P} = \sum_{ij} \boldsymbol{\Pi}_{i,j} (\boldsymbol{S}_i \cdot \boldsymbol{S}_j)$. Here the vector $\boldsymbol{\Pi}_{i,j}$ is nonzero since the inversion symmetry is absent at the center of the Mn-O-Mn bond because of the orthorhombic lattice distortion and/or the staggered $d_{3x^2-r^2}/d_{3y^2-r^2}$ orbital ordering. More concretely, because of the zigzag Mn-O chain, $\boldsymbol{P} = (P_a, P_b, P_c)$ is given by

$$P_\gamma = \Pi_\gamma \sum_i [(-1)^{i_x+i_y+m} \boldsymbol{S}_i \cdot \boldsymbol{S}_{i+\hat{x}} + (-1)^{i_x+i_y+n} \boldsymbol{S}_i \cdot \boldsymbol{S}_{i+\hat{y}}], \tag{1}$$

where $(m, n) = (0, 0)$ for $\gamma = a$, $(m, n) = (1, 0)$ for $\gamma = b$, and $(m, n) = (i_z + 1, i_z + 1)$ for $\gamma = c$. This contribution cancels out in the ground state due to the symmetry, but the dynamical fluctuations of $\boldsymbol{P}$ contribute to the electromagnon excitation. Especially, in the noncollinear ground state, the single magnon processes at the zone edge originate from Eq. (1). However, this scenario cannot explain the low-energy peak at ~2–3 meV (see insets of Fig. 2), which is comparable to or even larger than the high-energy peak at ~5–8 meV in $\mathrm{DyMnO_3}$ [12], $\mathrm{TbMnO_3}$ [16], and $\mathrm{Eu_{1-x}Y_xMnO_3}$ [17]. Therefore, the puzzle still remains.

A clue to this issue is the proximity to collinear spin phases, i.e., the A-type and E-type phases. Near the phase boundary, the spin configuration is subject to the significant deviation from a pure spiral with uniform spin rotation angles and contains higher harmonics [7,18], which is sensitively enhanced by the tiny spin-phonon coupling or by the weak magnetic anisotropy. In this Letter, we study the role of this higher harmonics on the electromagnon excitation, and resolve the puzzle of the OS in the terahertz-frequency regime.

We start with a realistic spin model for the Mn perovskites [7]. The model is basically a classical Heisenberg model on a cubic lattice, which contains the frustrating spin exchanges, the DM interaction, the single-ion spin anisotropies, and the biquadratic interaction. The Mn spins are treated as classical vectors. The Hamiltonian consists of five terms as $\mathcal{H} = \mathcal{H}_{\rm ex} + \mathcal{H}^{D}_{\rm sia} + \mathcal{H}^{E}_{\rm sia} + \mathcal{H}_{\rm DM} + \mathcal{H}_{\rm biq}$, with

$$\mathcal{H}_{\rm ex} = \sum_{\langle i,j\rangle} J_{ij} \boldsymbol{S}_i \cdot \boldsymbol{S}_j, \tag{2}$$

$$\mathcal{H}^{D}_{\rm sia} = D \sum_i S^2_{\zeta i}, \tag{3}$$

$$\mathcal{H}^{E}_{\rm sia} = E \sum_i (-1)^{i_x + i_y} (S^2_{\xi i} - S^2_{\eta i}), \tag{4}$$

$$\mathcal{H}_{\rm DM} = \sum_{\langle i,j\rangle} \boldsymbol{d}_{ij} \cdot (\boldsymbol{S}_i \times \boldsymbol{S}_j), \tag{5}$$

$$\mathcal{H}_{\rm biq} = -B_{\rm biq} \sum^{ab}_{\langle i,j\rangle} (\boldsymbol{S}_i \cdot \boldsymbol{S}_j)^2, \tag{6}$$

where i_x, i_y, and i_z represent coordinates of the ith Mn ion with respect to the cubic x, y, and z axes. For the a, b, and c axes, we adopt the $Pbnm$ notation [see Fig. 1(a)]. The first term $\mathcal{H}_{\rm ex}$ describes the superexchange interactions as shown in Fig. 1(a). The frustration between ferromagnetic J_{ab} and antiferromagnetic J_b in the ab plane results in a spiral spin order, while the interplane antiferromagnetic J_c causes a staggered stacking along the c axis. The terms $\mathcal{H}^{D}_{\rm sia}$ and $\mathcal{H}^{E}_{\rm sia}$ stand for the single-ion anisotropies. $\mathcal{H}^{D}_{\rm sia}$ makes the magnetization along the c axis hard. On the other hand, $\mathcal{H}^{E}_{\rm sia}$ causes an alternate arrangement of the local hard and easy magnetization axes in the ab plane due to the staggered orbitals. The term $\mathcal{H}_{\rm DM}$ denotes the DM interaction. The DM vectors $\boldsymbol{d}_{ij}$ associated with Mn-O-Mn bonds are expressed using five DM parameters because of the crystal symmetry [19]; α_{ab}, β_{ab}, and γ_{ab} for $\boldsymbol{d}_{ij}$ on the in-plane bonds, while α_c and β_c for $\boldsymbol{d}_{ij}$ on the interplane bonds. The last term $\mathcal{H}_{\rm biq}$ represents the biquadratic interaction working between adjacent two spins in the ab plane, which originates from the spin-phonon coupling [8]. We have microscopically determined the values of J_{ab}, J_b, J_c, D, and E [7]. The value of $B_{\rm biq}$ is determined so as to reproduce the relative intensities of two peaks in the experimental OS, while the DM parameters are tuned within the range of uncertainty of the estimates in Ref. [7].

We perform calculations using two sets of the model parameters (A and B) as (A) $J_{ab} = -0.74$, $J_b = 0.74$, $J_c = 1.2$, $(\alpha_{ab}, \beta_{ab}, \gamma_{ab}) = (0.1, 0.1, 0.16)$, $(\alpha_c, \beta_c) = (0.4, 0.1)$, $D = 0.24$, $E = 0.3$, and $B_{\rm biq} = 0.025$, and (B) $J_{ab} = -0.7$, $J_b = 0.99$, $J_c = 1.0$, $(\alpha_{ab}, \beta_{ab}, \gamma_{ab}) = (0.1, 0.1, 0.14)$, $(\alpha_c, \beta_c) = (0.45, 0.1)$, $D = 0.22$, $E = 0.25$, and $B_{\rm biq} = 0.025$. Here the energy unit is meV. These parameter sets give the ab plane spin-spiral propagating along the b axis with 6 times periodicity ($q_b = \pi/3$) and the bc-plane one with 5 times periodicity ($q_b = 2\pi/5$), respectively. The former spin state resembles the ab-plane spiral in $Eu_{1-x}Y_xMnO_3$ ($x = 0.45$) with $q_b \sim 0.3\pi$, while the latter resembles the bc-plane spiral in $DyMnO_3$ with $q_b = 0.39\pi$. Note that we adopt the commensurate spin states for convenience of the finite-size calculations, whereas the actual spin states are incommensurate. However, conclusions of this Letter are never affected by this difference. Sizes of the systems used for calculating the optical (magnon-dispersion) spectra are $18 \times 18 \times 6$ ($54 \times 54 \times 6$) and $20 \times 20 \times 6$ ($60 \times 60 \times 6$) along x, y, and z axes for respective cases, which match the periodicities of the spirals.

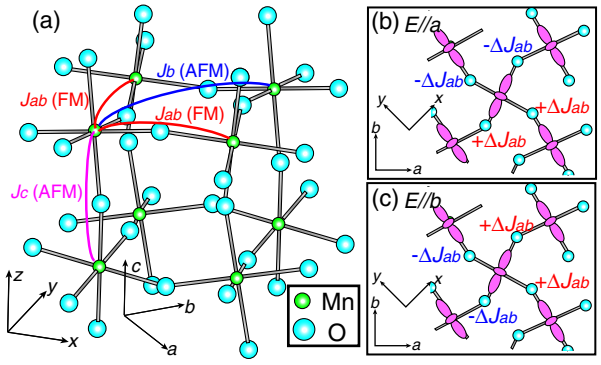

FIG. 1 (color online). (a) Superexchange interactions in RMnO$_3$ described by the Hamiltonian Eq. (2). (b) Modulations of the in-plane nearest-neighbor ferromagnetic exchanges under $\boldsymbol{E} \parallel a$. (c) Those under $\boldsymbol{E} \parallel b$. Here FM and AFM denote ferromagnetic and antiferromagnetic exchanges, respectively.

We study the electromagnon and magnon excitations by numerically solving the Landau-Lifshitz-Gilbert equation using the fourth-order Runge-Kutta method. The equation is given by

$$\frac{\partial \boldsymbol{S}_i}{\partial t} = -\boldsymbol{S}_i \times \boldsymbol{H}^{\rm eff}_i + \frac{\alpha_G}{S} \boldsymbol{S}_i \times \frac{\partial \boldsymbol{S}_i}{\partial t}, \tag{7}$$

where α_G (=0.1–0.2) is the dimensionless Gilbert-damping coefficient. We derive an effective local magnetic field $\boldsymbol{H}^{\rm eff}_i$ acting on the ith Mn spin $\boldsymbol{S}_i$ from the Hamiltonian $\mathcal{H}$ as $\boldsymbol{H}^{\rm eff}_i = -\partial \mathcal{H} / \partial \boldsymbol{S}_i$. A neutron-scattering experiment revealed strong reduction of the Mn spin moment at finite temperatures [18]. Thus we set the norm of the spin vector $|\boldsymbol{S}_i| = 1.4$.

For the origin of the electromagnon excitation, we consider the coupling $-\boldsymbol{E} \cdot \boldsymbol{P}$ between the external electric

field $\boldsymbol{E}$ and the spin-dependent $\boldsymbol{P}$ given by Eq. (1). Noticeably this coupling effectively modulates the nearest-neighbor ferromagnetic exchanges in the ab plane from $J_{ab}\boldsymbol{S}_i \cdot \boldsymbol{S}_j$ to $(J_{ab} - \boldsymbol{E} \cdot \boldsymbol{\Pi}_{ij})\boldsymbol{S}_i \cdot \boldsymbol{S}_j$. More concretely, the application of $\boldsymbol{E} \parallel a$ [$\boldsymbol{E} \parallel b$] corresponds to modulations of the in-plane spin exchanges shown in Fig. 1(b) [Fig. 1(c)].

Starting with spin configurations obtained in the Monte Carlo thermalization [7], we further relax them by the sufficient time evolution. Then we apply the electric field $\boldsymbol{E} \parallel a$ or $\boldsymbol{E} \parallel b$ as a short pulse at $t = 0$, and trace the time evolution of $\boldsymbol{P}$ given by Eq. (1). The electromagnon spectrum Im $\varepsilon(\omega)$ is calculated from the Fourier transformation of $\boldsymbol{P}(t)$.

In Fig. 2, we depict calculated electromagnon spectra for the cases of (a) ab-plane spiral state with parameter set A and (b) bc-plane spiral state with parameter set B. Irrespective of the spiral-plane orientation, large spectral weight emerges at low energy when $\boldsymbol{E} \parallel a$. In contrast, we observe no response to $\boldsymbol{E} \parallel b$ for both cases in agreement with the experiment [13]. For comparison, we display the experimental spectrum of $Eu_{0.55}Y_{0.45}MnO_3$ [17] and that of $DyMnO_3$ [12] in the insets. For both cases, we obtain fairly good agreement between theory and experiment. In the following, we discuss the results for the ab-plane spiral case. Similar discussion can be repeated for the bc-plane spiral case.

To identify origin of the two-peak structure of the electromagnon spectrum, we calculate electromagnon spectra and magnon-dispersion spectra along $\boldsymbol{k} = (0, k_b, 0)$, for various cases of interactions (see Fig. 3). The magnon spectra are calculated from the Fourier transformation of the space- and time-domain simulation data for the spin dynamics of $\delta S \parallel$ (ab spiral plane) after applying H as a short pulse to a single-site spin in the ab-spiral ground state. When the Hamiltonian consists of only the spin-exchange term and the single-ion anisotropy D term, i.e., $\mathcal{H}_{\rm ex}$ and $\mathcal{H}^{D}_{\rm sia}$ [see Fig. 3(a)], the spin spiral has uniform rotation angles. In practice, for the case of pure spiral order, translational symmetry is conserved upon the one lattice-unit translation if it is accompanied by an appropriate rotation of the spin axes. Then despite the long-period magnetic structure, matrix elements which mix magnon branches do not exist. In this case, we can see only one peak at a rather high energy of ~8 meV corresponding to that in Fig. 3(a). Incorporation of the DM interaction $\mathcal{H}_{\rm DM}$ does not change the spectral shape [see Fig. 3(b)].

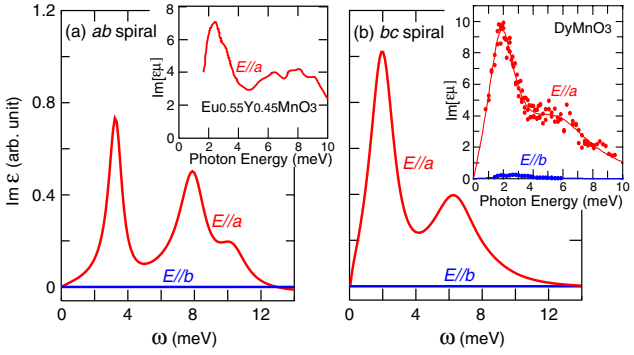

FIG. 2 (color online). Calculated electromagnon optical spectra for (a) ab-plane spiral state ($q_b = \pi/3$) with parameter set A, and (b) bc-plane spiral state ($q_b = 2\pi/5$) with parameter set B. Values of α_G used in the calculations are 0.1 and 0.2 for (a) and (b), respectively. Insets show the experimental spectra of $Eu_{0.55}Y_{0.45}MnO_3$ [17] and $DyMnO_3$ [12], respectively.

Further adding the single-ion anisotropy E term $\mathcal{H}^{E}_{\rm sia}$ gives rise to folding and anticrossing of the magnon dispersions. Namely, in the extended Brillouin zone picture, magnon branches separated by a multiple of the reciprocal lattice vector $\boldsymbol{G} = (0, q_b, 0)$ are mixed with each other where $q_b = \pi/3$ in the present case. This gives rise to changes in the spectral shape, i.e., another peak of the OS at a lower energy of ~3 meV appears, and the higher-lying peak slightly splits into two peaks as shown in Fig. 3(c). Finally we can see dramatic enhancement of the lower-lying peak in the OS when the Hamiltonian is full including the biquadratic term $\mathcal{H}_{\rm biq}$ as shown in Fig. 3(d). Strong magnon anticrossing causes rather flat magnon dispersions. The magnon branches predicted here would be observed experimentally.

We can see vital roles of the single-ion anisotropy $\mathcal{H}^{E}_{\rm sia}$ and the biquadratic interaction $\mathcal{H}_{\rm biq}$ in Figs. 4(a) and 4(b),

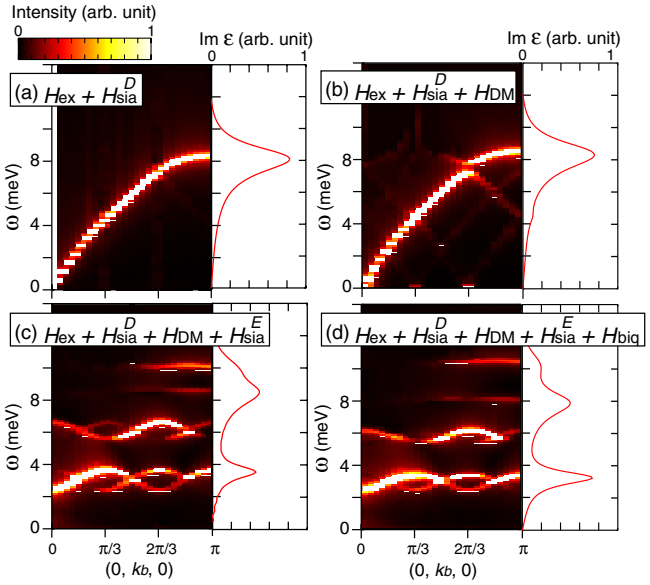

FIG. 3 (color online). Calculated intensity map of magnon (left panel) and electromagnon OS (right panel) for each Hamiltonian with successively adding the interactions. (a) $\mathcal{H}_{\rm ex} + \mathcal{H}^{D}_{\rm sia}$ giving a spin-spiral with uniform rotation angles. (b) Adding $\mathcal{H}_{\rm DM}$ induces negligibly small changes. (c) Incorporation of $\mathcal{H}^{E}_{\rm sia}$ causes the spin-angle modulation or higher harmonics of the spin-spiral, resulting in the magnon foldings and evolution of the lower-energy peak in the OS. (d) For full Hamiltonian including also $\mathcal{H}_{\rm biq}$, the lower-energy peak in the OS is further enhanced.

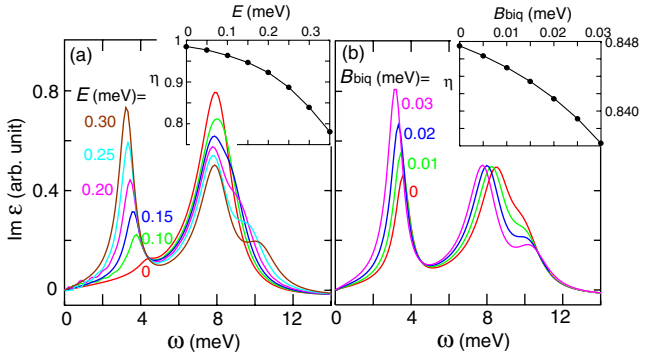

FIG. 4 (color online). Calculated electromagnon spectra for various strength of (a) single-ion anisotropy E and (b) biquadratic interaction B_{biq}. Insets show calculated η for the ab-plane spin spiral as functions of E and B_{biq}, respectively (see text). The value of B_{biq} [E] for (a) [(b)] is fixed at 0.025 [0.3].

which show the calculated spectra for various values of E and B_{biq}, respectively. Surprisingly the lower-lying peak is enhanced strongly by the weak anisotropy or by the tiny biquadratic interaction. In the insets of Figs. 3(a) and 3(b), we show the calculated ratio of the correlation functions of the a-axis and b-axis spin components at $\boldsymbol{q}_b$, $\eta = \sqrt{\hat{S}_a(\boldsymbol{q}_b)/\hat{S}_b(\boldsymbol{q}_b)}$, which is a measure for the deviation from a uniformly rotating spiral [7]. We see that the enhancement of the low-lying peak is accompanied by the decrease of η. Note that the deviation from the pure spiral is more significant when η is decreased more from unity. This indicates that the origin of the low-energy peak is the spin-angle modulation of the spin spiral. We indeed confirm that the two electromagnon resonances correspond to the magnons at $q_b = \pi$ and $q_b = \pi - 2q_b$ due to the form factor of Eq. (1) and the higher-harmonic spin components with $k = 2q_b$. These momenta coincide with the recent twin-magnon model [20], but we emphasize an important difference: Our theory is based on an anharmonic ground state whereas the twin model assumes a harmonic ground state and an anisotropy of the ME coupling in the spin space.

Let us now discuss the R dependence of the electromagnon spectra of $R\mathrm{MnO_3}$. In $\mathrm{TbMnO_3}$, the spectrum has more weight at the higher-energy peak [16], while in $\mathrm{DyMnO_3}$ with a smaller ionic R-site radius (r_R), the spectral weight is shifted to lower energy [12]. In the systematic study of $\mathrm{Eu_{1-x}Y_xMnO_3}$, transfer of the spectral weight to lower energies has been reported as the Y content x is increased (or as the averaged r_R is decreased) [16]. Note that with decreasing r_R, we approach the E-type phase, which results in a stronger influence of the biquadratic interaction. So far, the magnon spectrum in $R\mathrm{MnO_3}$ with a spiral spin order has only been reported for $\mathrm{TbMnO_3}$ [21]. In the compounds closer to the E-type phase, we expect that the magnon spectrum exhibits significant foldings. Further experimental data for these compounds are necessary to examine our theory.

In some of the $R\mathrm{MnO_3}$ compounds, deviation of frequencies between the magnetic resonance and the electromagnon has been reported [22]. This is natural because the magnetic resonance occurs at the zone center $\boldsymbol{k} = \boldsymbol{0}$ whereas the lower-lying electromagnon at $\boldsymbol{k} = (0, \pi - 2q_b, 0)$. Although their energies are close due to the flattened magnon-dispersion, they should be different.

In summary, we have studied the electromagnon dynamics taking into account all the relevant interactions and anisotropies in the spin Hamiltonian for $R\mathrm{MnO_3}$. It is found that the higher harmonics of the ground-state spiral spin configuration has crucial influences on the foldings of the magnon dispersion and also the electromagnon spectrum, which resolves the puzzle of the low-energy peak in the OS.

The authors are grateful to N. Kida, S. Miyahara, Y. Takahashi, J. S. Lee, M. P. V. Stenberg, and Y. Tokura for discussions. This work was supported by Grants-in-Aid (19048015, 19048008, 21244053, and 17105002), Funding Program for World-Leading Innovative R&D on Science and Technology (FIRST), and NAREGI Project from MEXT, Japan.

*mochizuki@erato-mf.t.u-tokyo.ac.jp

[1] For recent reviews, see Y. Tokura, Science **312**, 1481 (2006); J. Magn. Magn. Mater. **310**, 1145 (2007).
[2] T. Kimura *et al.*, Nature (London) **426**, 55 (2003).
[3] H. Katsura, N. Nagaosa, and A. V. Balatsky, Phys. Rev. Lett. **95**, 057205 (2005).
[4] M. Mostovoy, Phys. Rev. Lett. **96**, 067601 (2006).
[5] I. A. Sergienko and E. Dagotto, Phys. Rev. B **73**, 094434 (2006).
[6] G. A. Smolenski and I. E. Chupis, Usp. Fiziol. Nauk **137**, 415 (1982) [Sov. Phys. Usp. **25**, 475 (1982)].
[7] M. Mochizuki and N. Furukawa, J. Phys. Soc. Jpn. **78**, 053704 (2009); Phys. Rev. B **80**, 134416 (2009).
[8] T. A. Kaplan, Phys. Rev. B **80**, 012407 (2009).
[9] A. Pimenov *et al.*, Nature Phys. **2**, 97 (2006).
[10] A. Pimenov *et al.*, Phys. Rev. B **74**, 100403(R) (2006).
[11] H. Katsura, A. V. Balatsky, and N. Nagaosa, Phys. Rev. Lett. **98**, 027203 (2007).
[12] N. Kida *et al.*, Phys. Rev. B **78**, 104414 (2008).
[13] N. Kida, Y. Yamasaki, R. Shimano, T. Arima, and Y. Tokura, J. Phys. Soc. Jpn. **77**, 123704 (2008).
[14] R. Valdes Aguilar *et al.*, Phys. Rev. Lett. **102**, 047203 (2009).
[15] S. Miyahara and N. Furukawa, arXiv:0811.4082.
[16] Y. Takahashi *et al.*, Phys. Rev. Lett. **101**, 187201 (2008).
[17] Y. Takahashi *et al.*, Phys. Rev. B **79**, 214431 (2009).
[18] T. Arima *et al.*, Phys. Rev. Lett. **96**, 097202 (2006).
[19] For a symmetry analysis, see I. Solovyev, N. Hamada, and K. Terakura, Phys. Rev. Lett. **76**, 4825 (1996).
[20] M. P. V. Stenberg and R. de Sousa, Phys. Rev. B **80**, 094419 (2009).
[21] D. Senff *et al.*, Phys. Rev. Lett. **98**, 137206 (2007).
[22] N. Kida *et al.*, J. Opt. Soc. Am. B **26**, A35 (2009).